Neutron studies of magnetic oxide thin films

2008 J. Phys.: Condens. Matter 20 264009

(http://iopscience.iop.org/0953-8984/20/26/264009)

IOP PUBLISHING JOURNAL OF PHYSICS: CONDENSED MATTER

J. Phys.: Condens. Matter **20** (2008) 264009 (8pp) doi:10.1088/0953-8984/20/26/264009

Neutron studies of magnetic oxide thin films

Frédéric Ott

Laboratoire Léon Brillouin CEA/CNRS UMR 12, Centre d'Etudes de Saclay, 91191 Gif sur Yvette, Cedex, France

E-mail: Frederic.Ott@cea.fr

Received 15 October 2007, in final form 19 November 2007
Published 9 June 2008
Online at stacks.iop.org/JPhysCM/20/264009

Abstract

We describe the use of neutron scattering techniques such as reflectivity and diffraction for the study of oxide thin films. We first describe how neutron reflectivity can complement x-ray reflectivity for the study of some oxide materials. We then emphasize magnetic thin films which have become an important field of study in the 1990s, following the discovery of new phenomena in heterostructures: magnetic exchange coupling, exchange bias coupling at antiferro/ferromagnetic interfaces, enhanced magnetism in ultrathin films or tunnel magnetoresistance for example. We show how neutron scattering can provide detailed quantitative information about the magnetization depth profiles of thin films and about the magnetic order in epitaxial films.

(Some figures in this article are in colour only in the electronic version)

1. Introduction

During the early 1980s, advanced techniques for the deposition of ultrathin films were developed. This led to the fabrication of new artificial materials comprising the stacking of different materials in thin sandwiches (heterostructures). The combination of different types of materials gave rise to new physical phenomena: magnetic exchange coupling in rare-earth [1] and metallic superlattices [2–6] (figure 1(a)), exchange bias coupling at antiferro/ferromagnetic interfaces (figure 1(b)) [7–9], enhanced magnetism in ultrathin films [10], giant magnetoresistance in metallic spin valves [11] or tunnel magnetoresistance [12] (figure 1(c)).

Neutron reflectometry is a relatively new technique [13, 14] which developed in parallel with the fabrication of these new systems. Owing to the large magnetic coupling between the neutron and the magnetic moments, neutron reflectometry emerged as a powerful tool for obtaining information about the magnetic configurations in these systems. In the early studies, reflectivity was used to probe the ferromagnetism of metallic layers. Even though oxide layers were part of the heterostructures, especially in exchange bias systems such as pinning layers or in tunnel junctions as tunnel barriers, they were not directly characterized by neutron scattering.

However, since the late 1990s, more and more studies have been devoted to the study of oxide layers. It appeared that some oxide materials were likely to have high spin polarization which could make them candidate materials for use in devices using spin injection. Manganese oxide perovskites, which can be ferromagnetic, as well as more classical ferrites started to be deposited as thin films. These materials were used in magnetic tunnel junctions ($ABMnO_3$ perovskites [15] or Fe_3O_4 [16] as injection electrodes, or $CoFe_2O_4$ as a ferromagnetic tunnel barrier).

After the early studies of Eu based magnetic semiconductors (EuO and EuS) in the 1970s, the field was dormant until GaMnAs magnetic semiconductors were synthesized in the middle of the 1990s. Since then, a number of new systems have been synthesized in order to find room temperature magnetic semiconductors. The discovery of a suitable material could boost the field of spintronics. These new materials range from diluted semiconductors (GaMnAs) to magnetically doped insulating oxide materials (ZnO:Co, TiO_2:Co).

We can also mention studies performed on high T_c superconductors such as the penetration of the magnetic flux in superconductor thin films [17] or the proximity effects between magnetism and superconductivity [18].

In a first part, we will describe the technique of polarized neutron reflectivity. The use of this technique will then be illustrated with several studies on non-magnetic and on

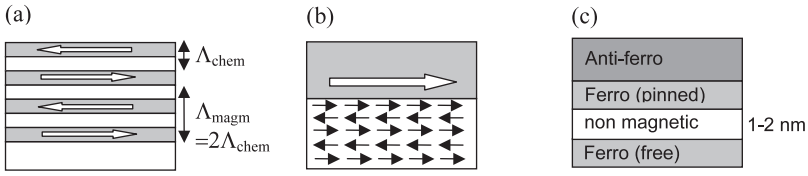

Figure 1. (a) Exchanged coupled superlattice with an antiferromagnetic order; (b) exchange bias between a ferromagnet and an antiferromagnet; (c) GMR system or magnetic tunnel junction.

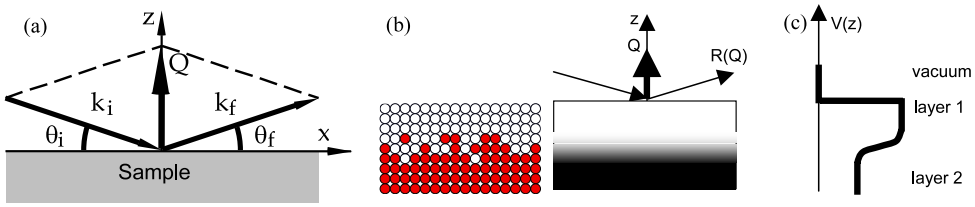

Figure 2. (a) Specular reflectivity geometry. The reflection angle is equal to the incidence angle; the scattering wavevector Q is perpendicular to the sample surface. (b) Interface between two surfaces. In the optical approximation, the interface is approximated as a continuous medium. (c) Reflection on a thin film deposited on a surface. The reflectivity measures the Fourier transform of the interaction potential $V(z)$.

magnetic systems. We will finish by showing that neutron diffraction can be used to probe antiferromagnetic oxide thin films.

2. Neutron reflectivity and polarized neutron reflectivity

2.1. Specular reflectivity

Neutrons can be reflected on surfaces in the same way as x-rays or electrons [19]. All the formalisms developed for x-ray reflectivity can be transposed to neutron reflectivity [20]. In a reflectivity geometry (figure 2(a)), the incidence angle θ_i on the surface is small (typically ranging from 0.5° to 5°). The reflection angle θ_r is the same as the incidence angle θ_i. As a consequence, the scattering wavevector $\boldsymbol{Q}$ is perpendicular to the surface. The typical neutron wavelengths are in the range 2–20 Å. Thus the range of accessible scattering wavevectors $\boldsymbol{Q} = \boldsymbol{k}_f - \boldsymbol{k}_i$ is in the range 0.05–3 nm^{-1}. This corresponds in real space to typical length scales between 2 and 100 nm. Neutron reflectivity is thus a technique adapted for the study of thin films but does not probe structures at the atomic level. In a reflectivity geometry it is possible to do the 'optical approximation' [20] and to model the neutron interaction with the material as a continuous potential. The details of the atomic structure are smoothed out (figure 2(b)). The interaction potential V with a material is given by

$$V = \frac{h^2}{2\pi m}\rho \qquad \text{with } \rho = \sum_i N_i b_i \tag{1}$$

where h is the Planck constant and m is the neutron mass; ρ is called the 'scattering length density' and is the sum of the atomic density of the nuclei in the material N_i multiplied by their individual nuclear scattering lengths b_i.

In the case of a magnetic system, the interaction between the neutron spin and the material magnetization is of the form $V = -\boldsymbol{\mu} \cdot \boldsymbol{B}$ where $\boldsymbol{\mu}$ is the neutron magnetic moment and $\boldsymbol{B}$ is the magnetic induction inside the thin film. One must note that neutrons are only sensitive to the magnetic induction and thus cannot distinguish between spin and orbital moment.

Table 1. Nuclear and magnetic optical index $n = 1 - \delta_N \pm \delta_M$ for some materials at $\lambda = 0.4$ nm.

Element	δ_N (10^{-6})	δ_M (10^{-6})
Fe	20.45	12.8
Co	5.7	10.5
Ni	24	3.8
Gd	5.0	14.5
$La_{0.7}Sr_{0.3}MnO_3$	9.4	4.4

In the reflectivity geometry, the equivalent of a neutron 'optical index' can be derived from the Schrödinger equation [20]. Neglecting absorption, the value of this optical index is given by the following expression:

$$n^{\pm} \approx 1 - \delta_N \pm \delta_M = 1 - \frac{\lambda^2}{2\pi}\rho \pm \frac{m\lambda^2}{h^2}\mu \cdot B \tag{2}$$

where δ_N is the nuclear contribution to the optical index, and δ_M is the magnetic contribution to the optical index, the sign of the magnetic contribution depends on the relative orientation of the neutron spin with respect to the magnetization (parallel or antiparallel). Table 1 gives values of optical indexes for some typical materials. One should notice that the magnetic optical index is of the same order of magnitude as the nuclear optical index. Both optical indexes n^+ and n^- can be measured by using polarized neutrons and thus detailed information about the magnetic structure of the sample can be obtained.

In a specular reflectivity measurement, it is assumed that there are no inhomogeneities along the film surface. Thus the interaction potential V is only a function of the depth z in the multilayer system (figure 2(c)). In a first approximation, the specular reflectivity measures the Fourier transform of the optical index profile $n(z)$.

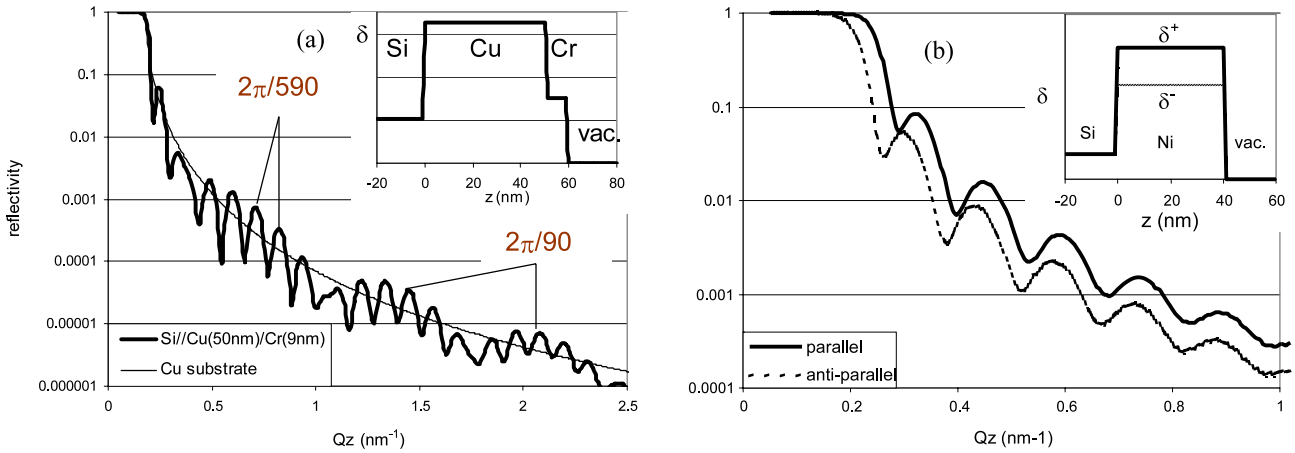

Figure 3. (a) Reflectivity on a multilayer system Si ‖ Cu(50 nm)/Cr(9 nm). The short period oscillations are characteristic of the total thickness of the layer (59 nm); the long range modulation is characteristic of the thin Cr layer (9 nm). Inset: optical index profile as a function of the depth in the film. (b) Reflectivity of a magnetic film Si ‖ Ni(40 nm). The reflectivity depends on the relative orientation of the neutron spin with respect to the magnetization. Inset: optical index profile for both neutron polarizations (parallel and antiparallel).

However, at low incidence angles, there is total reflection up to a critical wavevector $Q_c = 4\sqrt{\pi\rho}$ and thus the Born approximation is not valid at small scattering wavevectors. The Born approximation can be applied only above a scattering wavevector of about $3Q_c$. Below this limit, one must solve the Schrödinger equation and perform a full dynamical calculation. The detailed theoretical treatment of the polarized reflectivity can be found in [20–24]. Figure 3(a) presents the situation of the reflection of a neutron beam on a multilayer Si ‖ Cu/Cr: above the critical wavevector of total reflection, the reflected intensity decreases as $1/Q^4$. Modulations of the reflected intensities are observed. They correspond to constructive and destructive interferences of the neutron waves scattered by the different interfaces of the multilayer system. These oscillations are called Kiessig fringes. Their pattern is characteristic of the multilayer system. Figure 3(b) presents the situation of a magnetic thin film on a substrate. In this case, the optical index depends on the relative orientation of the neutron spin with respect to the thin film magnetization. The measured reflectivity is very different for neutron incident with a spin parallel to the magnetization (optical index $n^+ = 1 - \delta_N + \delta_M$) and for neutrons incident with a spin antiparallel to the magnetization (optical index $n^- = 1 - \delta_N - \delta_M$).

The measure of the reflectivity probes the profile of optical index $n(z)$ along the normal (Oz) to the thin film system. Numerical models must be used to reconstruct the thickness of the different layers of the system as well as their individual scattering length densities which is characteristic of their chemical composition. Interdiffusion and roughness at interfaces can be quantified with more detailed models. In the case of magnetic systems, information on the amplitude and the direction of the magnetization of the different layers can be obtained using polarized neutrons. In practice, it is possible to measure four quantities in a polarized reflectivity experiment: two non-spin-flip reflectivities, R^{++} (resp. R^{--}), corresponding to the number of incoming 'up' (resp. 'down') neutrons reflected with an 'up' (resp. 'down') polarization; two spin-flip reflectivities, $R^{+-} = R^{-+}$, corresponding to the number of neutrons experiencing a spin-flip during the reflection on the sample. In a first approximation, the non-spin-flip signals probe the components of the magnetization which are parallel to the applied field; the spin-flip signals are sensitive to the component of the magnetization perpendicular to the applied field. Combining this information it is possible to reconstruct the magnetization direction and amplitude through the depth of the film. The depth resolution is of the order of 2–3 nm in simple systems. Among the advantages of polarized neutron reflectivity we can mention: (i) the very large and simple magnetic interaction, (ii) it is a surface technique and thus is not sensitive to paramagnetic or diamagnetic contribution from the substrate, (iii) there is no absorption, (iv) there are no phenomenological parameters. All these characteristics make neutron reflectivity data easy to model and interpret.

2.2. Real experiments

One has to keep in mind that most existing reflectometers are designed to perform experiments on samples which have a surface of the order of 10 cm^2. In the case of optimized reflectometers with focusing systems (such as PRISM at the LLB), it is possible to perform experiments on samples which have a size of the order of 1 cm^2. These limitations in size imply that the studied samples need to have a very good homogeneity over a very large surface: the thickness of the layers needs to be homogeneous and the substrate needs to be flat over the whole sample surface. If this is not the case, only averages over the sample surface will be measured and the information that can be obtained about the sample will be limited.

The reflectivity signal drops very quickly with the scattering wavevector value. For a perfect interface, at large Q values, the reflectivity is proportional to $1/Q^4$. Q values of the order of 2–3 nm^{-1} typically correspond to reflectivity of

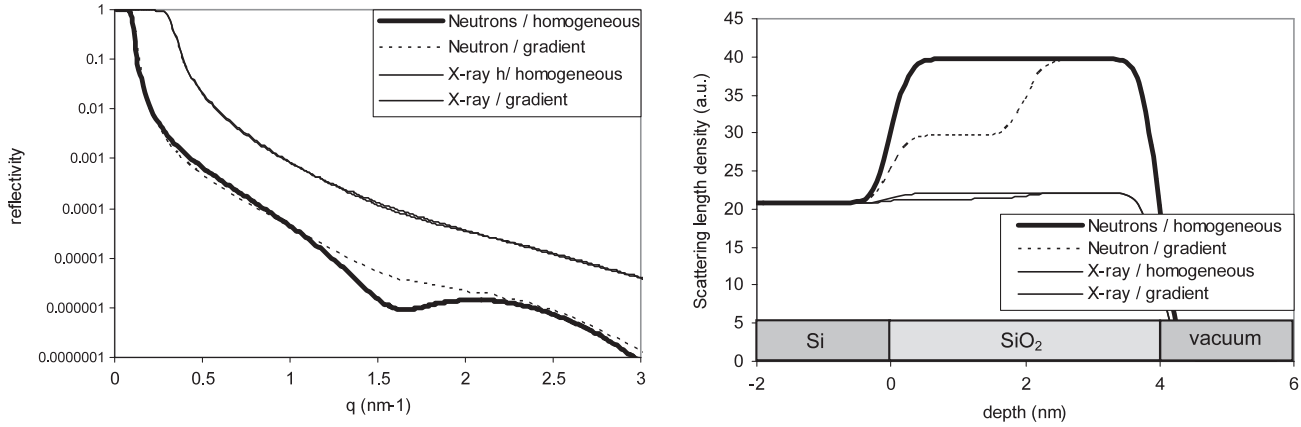

Figure 4. Comparison of the neutron reflectivity and the x-ray reflectivity on a SiO_2 ‖ Si structure. The contrast between the layers is much larger in the case of neutrons, leading to higher amplitude oscillations, which on the contrary are very small in the case of x-rays. Sub-structures in the oxide layer, due for example to an oxidation gradient, give measurable effects in neutron reflectivity.

Table 2. Optical indices of different oxides. Note the large difference between δ_{Si} and δ_{SiO2} in the case of neutrons.

Element	$\delta_{neutrons}(10^{-6})$	$\delta_{x-rays}(10^{-6})$
Si	5.3	7.6
SiO_2	10.1	8.11
SiC	13.3	10.43
Al	5.29	8.45
Al_2O_3	14.23	12.9

the order to 10^{-6} and require measuring times of the order of 2–6 h.

The absorption of neutrons is negligible in most materials. The typical penetration depth for materials such as silicon or aluminum is of the order of 50 mm (depending of the wavelength). This makes it easy to set up complex sample environments on neutron spectrometers. The available ancillary equipment includes: cryomagnets (temperature range 1.6–300 K; magnetic field range 0–7 T), furnaces (temperature up to 800 °C); closed liquid cells (made of quartz or silicon).

3. Neutron reflectivity studies

3.1. Probing oxide layers

Neutron reflectivity can be used to probe oxide layers since the neutron optical index of oxides are usually very different from non-oxidized materials (table 2) [25]. This makes neutron reflectivity much more sensitive to details in an oxide structure than x-ray reflectivity.

For example, the preparation of SiO_2 oxide films on silicon substrates by three different methods (thermal, chemical and electrochemical oxidation) have been compared by Bertagna *et al* [26] (figure 4). Depending on the preparation method, the obtained films give very different reflectivity results. Anodic and chemical oxides are found to be not very dense (60–75% of the theoretical density). Thermal oxides are the densest (95%).

Neutron reflectivity may also be useful in the case of some specific materials such as boron which is strongly absorbing

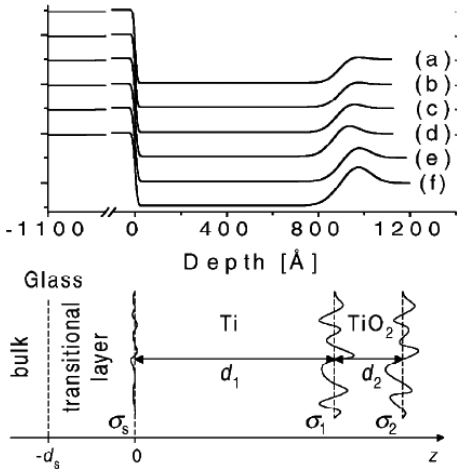

Figure 5. Oxidation profile as a function of the annealing time at the surface of a Ti film. (a) As prepared and annealed at (b) 150 °C for 60 min, (c) 200 °C for 30 min, (d) 250 °C for 20 min (e), 300 °C for 15 min and (f) 350 °C for 15 min. Adapted from [33].

neutrons (ex: the study of borophosphosilicate glass thin films used in microelectronic circuit devices [27]) or titanium which has a negative scattering length (such as TiO_x coatings for glazing [28–30]). Neutron reflectometry has sometimes been used to characterize the oxidation of metallic thin films [31–33] (figure 5).

Another key advantage of neutrons is their high sensitivity to D_2O (compared to x-rays). Neutron reflectivity has for example been used to characterize the moisture transport through Al_2O_3/polymer multilayered barrier films for flexible displays [34]. It has also been used to characterize the adsorption of water on hydrophobic/hydrophilic TiO_2 surfaces under UV illumination [35].

Another advantage which must be mentioned is that in neutron reflectometry it is easy to set up complex sample environments. This is especially true in the case of solid/liquid interfaces where the neutron beam can be sent through the substrate and probe the solid–liquid interface with negligible absorption [36–38].

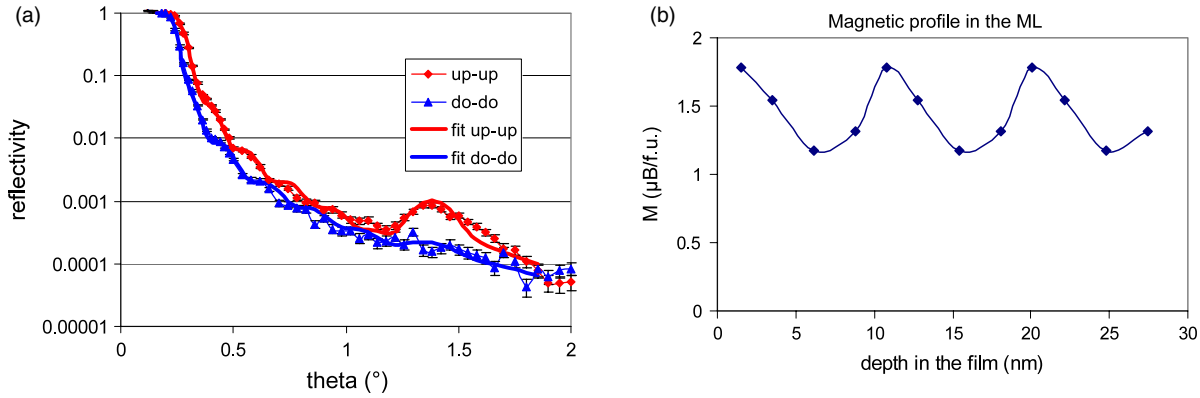

Figure 6. (a) Reflectivity on a superlattice $[(LaMnO_3)a/(SrMnO_3)b]_n$. (b) Magnetic profile in the superlattice.

4. Polarized neutron reflectivity studies

4.1. Superlattices

The first example illustrates the use of the magnetic contrast to measure the chemical segregation in manganite heterostructures: $[(LaMnO_3)a/(SrMnO_3)b]_n$ (with $8 < a < 12$; $4 < b < 8$ unit cells). These superlattices are deposited layer by layer in order to enforce a cationic order between La and Sr and a cationic segregation between Mn^{3+} and Mn^{4+}. The first material is antiferromagnetic in its bulk form, the second is ferromagnetic. The objective of the measurement was to check if the cationic segregation (La/Sr) effectively induced a (AF/F) stacking. The reflectivity on one of these systems is presented on figure 6(a). Around the angle $\theta = 1.3°$, a super-structure peak corresponding to the system's periodicity can be observed. The contrast between the two reflectivity curves 'up' and 'down' is characteristic of the in-depth magnetization profile. In order to model the reflectivity curves, it is only necessary to introduce a small modulation of the magnetization in the system (figure 6(b)): the cationic segregation does not lead to a clear magnetic segregation. The magnetization modulation is only 25% between the two types of layers.

4.2. Magnetic oxide thin films

Polarized neutron reflectivity has also been used to probe the magnetism of individual thin films of magnetic oxide layers (manganites [39, 40] or Fe_3O_4 [16–41]). We show here the use of the magnetic contrast to probe the structure of a multilayer in which the components are very close: iron oxides, Fe_2O_3 (antiferromagnetic) and Fe_3O_4 (magnetic). These oxides have an interest in the fabrication of magnetic tunnel junctions using spin polarized currents. The Fe_2O_3 layer is used as a pinning layer for the Fe_3O_4 electrode. The structure is presented on figure 7(a). X-ray reflectivity does not distinguish the two layers because the difference in optical index is of the order of 1%. For neutron reflectivity, the optical contrast is very large since one material is magnetic and the second is not. The expected stacking is described on figure 7. Surprisingly, instead of observing a clear segregation between the two layers, an oxido-reduction has taken place between the two layers. The Fe_2O_3 has been reduced and has turned magnetic; the Fe_3O_4 has been oxidized and has lost some of its magnetism. It must be noted that during the growth, RHEED diagrams indicate that the correct phases are growing. These oxido-reduction phenomena take place over timescales of the order of a week.

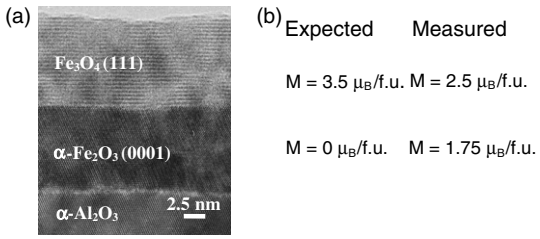

Figure 7. (a) Bilayer Fe_2O_3/Fe_3O_4. (b) Expected and measured magnetic profiles.

4.3. Manganites

The hysteresis cycle of $La_{0.7}Sr_{0.3}MnO_3$ thin films shows a region with a low coercivity on which is superimposed a contribution which requires 0.3 T to be saturated. This suggests that the films are not homogeneous and that they are composed of several phases having different coercivities. Neutron reflectivity measurements were performed on single $La_{0.7}Sr_{0.3}MnO_3$ thin films in order to probe the magnetization profiles through the depth of the films as a function of the temperature. Figure 8 shows the reflectivity on a 16 nm $La_{0.7}Sr_{0.3}MnO_3$. Modeling using a homogeneous magnetic layer does not provide satisfactory fits. In order to quantitatively model the data, it has been necessary to introduce a model taking into account different magnetizations at the interfaces. We considered a three layers model with magnetizations M_1, M_2 and M_3 in the depth of the films. Figure 9 shows the variations of the magnetizations M_1, M_2 and M_3 as a function of the temperature. One can note that the interface magnetization is reduced by 25–30%.

4.4. Superconductors—proximity effects

Since superconductivity and magnetism are closely related, polarized neutron reflectivity has been applied to the study of

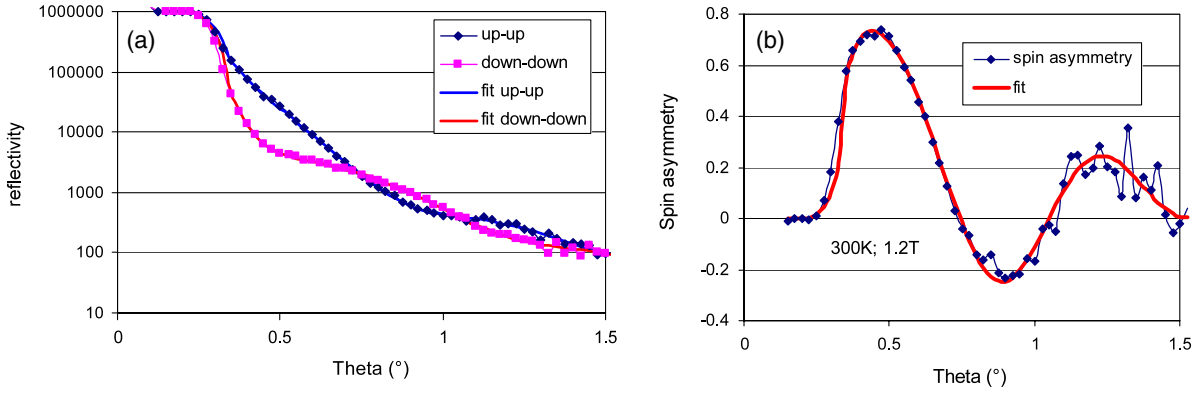

Figure 8. (a) Reflectivity of a $La_{0.7}Sr_{0.3}MnO_3$ (16 nm) film deposited on $SrTiO_3$. (b) Fitted spin asymmetry.

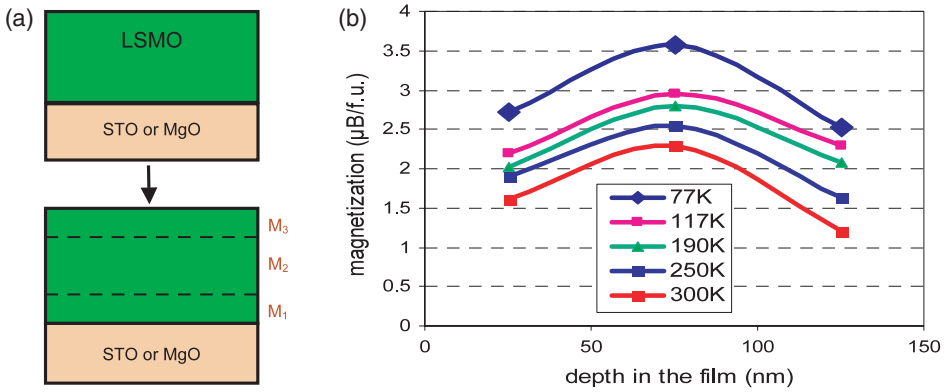

Figure 9. (a) Modeling of the system: (top) perfect system, (bottom) more realistic model. (b) Magnetization profiles as a function of the temperature for the system LSMO(16 nm) ‖ STO.

high T_c superconductor thin films and heterostructures. One of the first topics to be studied was the penetration of the magnetic flux and magnetic vortices in high T_c $YBa_2Cu_3O_7$ thin films [17–43].

A second topic which is presently of interest is the study of proximity effect in superconductor/magnetic heterostructures. Polarized neutron reflectivity has been applied to probe the interface between a superconductor and a magnetic layer in order to validate theoretical models [18–45]. It is suggested that an antiphase magnetic proximity coupling could exist where a ferromagnetic moment is induced in $YBa_2Cu_3O_7$ that is oriented antiparallel to the one in $La_{0.7}Ca_{0.3}MnO_3$ (figure 10, model 1). Another possibility is the existence of a ferromagnetic 'dead layer' either paramagnetic or antiferromagnetic within the $La_{0.7}Ca_{0.3}MnO_3$ region.

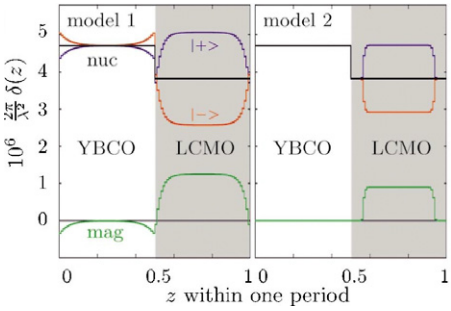

Figure 10. Model potentials that reproduce the experimental neutron reflectivity data measured on a $[LCMO(16\ nm)/YBCO(16\ nm)]_6$ heterostructure. Left: antiphase magnetic proximity effect; right: 'dead layer' model. $\delta(z) \sim V(z)$ is the deviation of the refractive index from 1, λ is the neutron wavelength. Adapted from [18].

5. Neutron diffraction

In the previous examples, we discussed experiments performed at grazing incidence. In this geometry, the interaction between the sample and the neutron beam is maximized but it limits the characterization to nanoscale ferromagnetic properties.

One of the unique features of neutron diffraction is that the magnetic order can be probed at the atomic scale [46]. As it has been mentioned above, the neutron magnetic scattering length is of the same order as the nuclear scattering length. Diffraction experiments can be performed with short wavelength neutrons (from 0.5 to 2.5 Å). It is thus possible to measure the magnetic structure factor of a crystal, that is the location of the magnetic atoms. Neutrons provide information about the absolute value of the magnetization but also about their directions (Fe moments in $YBa_2Fe_3O_8$ for example [47]). It is thus possible to unravel complex magnetic orders (antiferromagnetic, helicoidal or with several magnetic sublattices). It is also possible to measure the

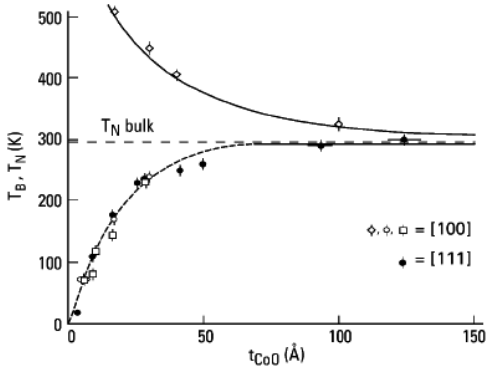

Figure 11. Measured CoO ordering temperatures, T_N (diamonds) and blocking temperatures T_B (squares and dots) are given versus the thickness of the CoO layer for a Fe_3O_4/CoO system. Note the divergence of the two curves, indicating that the measured reduction of T_B is not due to a reduction of the ordering temperature at low t_{CoO}. Adapted from [53].

magnetic form factors which gives the spatial distribution of the magnetic electrons. This permits to reconstruct spin density maps in magnetic crystals [48]. Following the dependence of the magnetic scattering as a function of the temperature can give fine information about magnetic phase transitions: spin reorientation phenomena [49] or the order parameter of magnetic sublattices (Er in $ErBa_2Cu_3O_7$ for example [50]).

The volume of magnetic matter is very small in thin films, but nevertheless, the performances of modern neutron spectrometers are such that high angle diffraction experiments can be performed on epitaxial thin films. Since the absorption is negligible, any direction in the reciprocal space can be probed and the sample substrate is not an issue, which is interesting compared to the use of x-rays. In practice, it is possible to probe epitaxial thin films with thicknesses down to 10 nm. Neutron diffraction is especially unique when probing antiferromagnetic crystals. Another advantage in the case of antiferromagnetic crystals is that it often gives rise to purely magnetic diffraction peaks which are not superimposed with structural peaks [51]. In the case of oxide films, the AF order in single layer NiO films as thin as 20 nm has been probed [52].

Neutron diffraction can be used in various situations for thin films. It has been used to follow the Néel transition temperature of thin films and correlate it with the apparition of exchange bias in systems such as Fe_3O_4/CoO. It has been demonstrated [53] that the blocking temperature at which the exchange coupling appears is not trivially correlated with the Néel temperature of the AF material (see figure 11). For very thin films (below 5 nm), while the blocking temperature drops, the Néel temperature increases significantly.

In [NiO/CoO] superlattices, the propagation of the antiferromagnetic order throughout the superlattice as a function of the thickness of the bilayer period (ranging from 4 to 9 nm) [54] was probed by neutron diffraction. Neutron diffraction can also be used to check the influence of epitaxial strain on the AF order in epitaxial films. For example, in CoO films, an epitaxial strain of 0.5% increases the Néel temperature by about 15 K [54]. This is a rather general trend. More recently, neutron diffraction showed that the epitaxial strain destroys the helical order in $BiFeO_3$ films [55]. This is an important piece of information since the knowledge of the magnetic order is a prerequisite for the understanding and use of magnetoelectric materials [56].

Beyond the information about the magnetic order, more refined information may be obtained about the sizes of AF domains by analyzing the diffraction peak widths. This information is of particular interest in exchange bias systems in which the antiferromagnetic microstructure is likely to play a key role in the exchange bias mechanism. This has been demonstrated in Fe_3O_4/NiO superlattices [57]. The field dependence of domains in the antiferromagnetic NiO is correlated with the presence or absence of exchange biasing. The data suggest that in this system, exchange biasing originates from domain walls frozen in the antiferromagnet upon field cooling.

Polarized grazing incidence diffraction geometry has been also been used [58, 59], but in practice, such experiments are much more difficult to set up and also prevent scanning in arbitrary directions in Q-space which in practice is essential, especially in the case of antiferromagnetic crystals.

6. Conclusion—the future

Neutron scattering offers several techniques that are direct probes of the magnetization in thin films. At a nanometric scale, the polarized neutron reflectivity technique is a good choice. The depth dependence of the magnetization can be probed. It can easily be used to measure antiferro-type, ferro-type or helical ordering in superlattices, probe complex magnetic ordering in multilayers, give detailed insights into problems such as the magnetism of ultrathin film or the bias exchange mechanism. The technique is now well established and a wealth of literature is available. A large number of neutron reflectometers are available across the world [60]. The Web site [61] gives you links to neutron reflectivity simulation and fitting programs. Current developments are connected to probing the lateral nanomagnetic and micromagnetic structures of thin films using off-specular [62, 63] or grazing incidence small angle scattering [64, 65]. These techniques are still in development and have rarely been applied to oxide layers.

One of the limitations of neutron reflectivity is that the technique is not element specific. Another issue is that the neutron fluxes are still low. Big efforts are being made to increase the flux on neutron reflectometers. Flux gains ranging from 10 to 100 can reasonably be expected in the next decade through the implementation of new types of neutron reflectometers. Quantitative gains in the measuring time and in the minimum sample size will be achieved.

At the atomic scale, diffraction experiments are possible on very small quantities of matter (down to 0.001 mm^3). Magnetic structures specific to thin film heterostructures (∼20–100 nm thick) can be characterized. Rapid progress is being made in this field through the use of high resolution position sensitive detectors on single crystal diffractometers which allow reducing the acquisition times by an order of magnitude: several diffraction peaks are measured at once, the shapes of the diffraction peaks are measured at

once and complex magnetic structures can be very quickly disentangled [66].

Other opportunities may appear in the next five years when new neutron spallation sources come into operation.

References

[1] Majkrzak C F *et al* 1988 *J. Appl. Phys.* **63** 3447–52
Majkrzak C F *et al* 1986 *Phys. Rev. Lett.* **56** 2700–3
[2] Grünberg P *et al* 1986 *Phys. Rev. Lett.* **57** 2442
[3] Schreyer A *et al* 1997 *Phys. Rev. Lett.* **79** 4914–7
[4] Langridge S *et al* 2000 *Phys. Rev. Lett.* **85** 4964–7
[5] Hjörvasson B *et al* 1997 *Phys. Rev. Lett.* **79** 901
[6] Huang Y Y, Felcher G P and Parkin S S P 1991 *J. Magn. Magn. Mater.* **99** 31–8
[7] te Velthuis S G E *et al* 2002 *Phys. Rev. Lett.* **89** 127203
te Velthuis S G E *et al* 2000 *J. Appl. Phys.* **87** 5046
te Velthuis S G E *et al* 1999 *Appl. Phys. Lett.* **75** 4174–6
[8] Radu F *et al* 2002 *J. Magn. Magn. Mater.* **240** 251–3
Radu F *et al* 2003 *Phys. Rev.* B **67** 134409
[9] Noguès J *et al* 1999 *J. Magn. Magn. Mater.* **192** 203–32
Fitzsimmons M R *et al* 2000 *Phys. Rev. Lett.* **84** 3986–9
Gierlings M *et al* 2002 *Phys. Rev.* B **65** 092407/1–4
[10] Baczewski L T *et al* 2006 *Phys. Rev.* B **74** 075417
[11] Baibich M N *et al* 1988 *Phys. Rev. Lett.* **61** 2472
[12] Miyazaki T and Tezuka N 1995 *J. Magn. Magn. Mater.* **139** L231–4
Moodera J S *et al* 1995 *Phys. Rev. Lett.* **74** 3273–6
[13] Majkrzak C F, Cable J W, Kwo J, Hong M, McWhan D B, Yafet Y and Waszcak J 1986 *Phys. Rev. Lett.* **56** 2700–3
[14] Felcher G P, Hilleke R O, Crawford R K, Haumann J, Kleb R and Ostrowski G 1987 *Rev. Sci. Instrum.* **58** 609–19
[15] Viret M *et al* 1997 *Europhys. Lett.* **39** 545–9
[16] Moussy J B *et al* 2004 *Phys. Rev.* B **70** 9
[17] Lauter-Pasyuk V *et al* 1998 *Physica* B **248** 166–70
[18] Stahn J *et al* 2005 *Phys. Rev.* B **71** 140509
Chakhalian J *et al* 2006 *Nat. Phys.* **2** 244–8
[19] Lekner J 1987 *Theory of Reflection of Electromagnetic and Particle Waves* (Dordrecht: Martinus Nijhoff)
[20] Fermon C, Ott F and Menelle A 1999 Neutron Reflectivity *X-Ray and Neutron Reflectivity: Principles and Applications* (*Springer Lecture Notes in Physics*) ed J Daillant and A Gibaud (Berlin: Springer) p 163
de Bergevin F 1999 *X-Ray and Neutron Reflectivity: Principles and Applications* (*Springer Lecture Notes in Physics*) ed J Daillant and A Gibaud (Berlin: Springer) p 3
[21] Felcher G P *et al* 1987 *Rev. Sci. Instrum.* **58** 609–19
[22] Blundell S J and Bland J A C 1992 *Phys. Rev.* B **46** 3391–400
[23] Fermon C, Miramond C, Ott F and Saux G 1996 *J. Neutron Res.* **4** 251
[24] Pleshanov Z 1994 *Physica* B **94** 233–43
[25] Dura J A, Richter C A, Majkrzak C F and Nguyen N V 1998 *Appl. Phys. Lett.* **73** 2131
[26] Bertagna V, Erre R and Saboungi M L *et al* 2004 *Appl. Phys. Lett.* **84** 3816–8
[27] Chen-Mayer H H, Lamaze G P, Coakley K J and Satija S K 2003 *Nucl. Instrum. Methods* A **505** 531
[28] Caccavale F, Coppola R, Menelle A, Montecchi M, Polato P and Principi G 1997 *J. Non-Cryst. Solids* **218** 291–5
[29] Battaglin C, Caccavale F, Menelle A, Montecchi M, Nichelatti E, Nicoletti F and Polato P 1999 *Thin Solid Films* **351** 176
[30] Battaglin G, Menelle A, Montecchi M, Nichelatti E and Polato P 2002 *Glass Technol.* **43** 203
[31] Wiesler D G and Majkrzak C F 1994 *Physica* B **198** 181
[32] Pusenkov V M, Moskalev K, Pleshanov N, Schebetov A, Syromyatnikov V, Ul'yanov V, Kobzev A and Nikonov O 2000 *Physica* B **276** 654
[33] Metelev S V, Pleshanov N K, Menelle A, Pusenkov V M, Schebetov A F, Soroko Z N and Ul'yanov V A 2001 *Physica* B **297** 122
[34] Vogt B D, Lee H J, Prabhu V M, DeLongchamp D M, Lin E K, Wu W L and Satija S K 2005 *J. Appl. Phys.* **97** 7
[35] Jribi R 2008 *Langmuir* submitted
[36] Tun Z, Noel J J and Shoesmith D W 1997 *Physica* B **241** 1107
[37] Tun Z, Noel J J and Shoesmith D W 1999 *J. Electrochem. Soc.* **146** 988
[38] Noel J J, Jensen H L, Tun Z and Shoesmith D W 2000 *Electrochem. Solid State Lett.* **3** 473
[39] Ott F, Viret M, Borges R, Lyonnet R, Jacquet E, Fermon C and Contour J P 2000 *J. Magn. Magn. Mater.* **211** 200
[40] Borges R P *et al* 2001 *J. Appl. Phys.* **89** 3868–73
[41] Morrall P, Schedin F, Langridge S, Bland J, Thomas M F and Thornton G 2003 *J. Appl. Phys.* **93** 7960
[42] Lauter-Pasyuk V, Lauter H J, Lorenz M, Aksenov V L and Leiderer P 1999 *Physica* B **268** 149
[43] Lauter-Pasyuk V, Lauter H J, Lorenz M, Petrenko A, Nikonov O, Aksenov V L and Leiderer P 2000 *Physica* B **276** 776
[44] Chakhalian J *et al* 2006 *Nat. Phys.* **2** 244–8
[45] Deen P P *et al* 2006 *Phys. Rev.* B **74** 224414
[46] Lynn J W 1994 *J. Appl. Phys.* **75** 6806
[47] Huang Q, Karen P, Karen V L, Kjekshus A, Lynn J W, Mighell A D, Rosov N and Santoro A 1992 *Phys. Rev.* B **45** 9611
[48] Aebersold M A *et al* 1998 *J. Am. Chem. Soc.* **120** 5238–45
[49] Piquer C *et al* 2004 *J. Appl. Phys.* **95** 6308–16
[50] Lynn J W, Clinton T W, Li W-H, Erwin R W, Liu J Z, Vandervoort K and Shelton R N 1989 *Phys. Rev. Lett.* **63** 2606
[51] Lind D M, Tay S P, Berry S D, Borchers J A and Erwin R W 1993 *J. Appl. Phys.* **73** 6886
[52] Doan T D, Hennion B and Ott F 2004 unpublished data
[53] van der Zaag P J, Ijiri Y, Borchers J A, Feiner L F, Wolf R M, Gaines J M, Erwin R W and Verheijen M A 2000 *Phys. Rev. Lett.* **84** 6102
[54] Borchers J A, Carey M J, Erwin R W, Majkrzak C F and Berkowitz A E 1993 *Phys. Rev. Lett.* **70** 1878
[55] Béa H, Bibes M, Petit S, Kreisel J and Barthelemy A 2007 *Phil. Mag. Lett.* **87** 165
[56] Béa H *et al* 2008 *Phys. Rev. Lett.* at press
[57] Borchers J A, Ijiri Y, Lind D M, Ivanov P G, Erwin R W, Qasba A, Lee S H, O'Donovan K V and Dender D C 2000 *Appl. Phys. Lett.* **77** 4187
[58] Doan T D *et al* 2003 *Physica* B **335** 72–6
[59] Doan T D *et al* 2002 *Appl. Phys.* A **74** S186–8
[60] http://material.fysik.uu.se/Group_members/adrian/reflect.htm
[61] http://neutronreflectivity.neutron-eu.net/main
[62] Felcher G P *et al* 1994 *Neutron News* **5** 18–22
[63] Langridge S *et al* 2000 *Phys. Rev. Lett.* **85** 4964–7
[64] Fermon C *et al* 1999 *Physica* B **267/268** 162–7
[65] Pannetier M, Ott F, Fermon C and Samson Y 2003 *Physica* B **335** 54–8
[66] Goukassov A *et al* 2008 at press